

First-principles study of the spin-lattice coupling in spin frustrated DyMn₂O₅

Tianqi Shen, Kun Cao, Guang-Can Guo, and Lixin He *
Key Laboratory of Quantum Information, University of Science and
Technology of China, Hefei, 230026, People's Republic of China
(Dated: November 29, 2018)

The lattice dynamic properties and spin-phonon coupling in DyMn₂O₅ are studied by using the density-functional theory. The calculated phonon frequencies are in very good agreement with experiments. We then compare the phonon modes calculated from different spin configurations. The results show that the phonon frequencies change substantially in different spin configurations, suggesting that the spin-phonon coupling in this material is very strong. Especially, the short range spin ordering has drastic effects on the highest Raman and IR phonon modes that might be responsible for the observed phonon anomalies near and above the magnetic phase transitions.

PACS numbers: 75.25.+z, 77.80.-e, 63.20.-e

I. INTRODUCTION

Manganese oxides including RMnO₃,^{1,2} and RMn₂O₅ (R=Tb, Dy, Ho, etc.)^{3,4,5} are a very special class of improper ferroelectrics that display strong magnetoelectric (ME) effects, such as the “colossal magnetodielectric” (CMD) effects and magneto-polarization-flop effects.^{1,2,6} These materials have attracted great attention,^{7,8,9,10} because the strong ME effects can be utilized to tune the electric properties of the materials via applied magnetic field, or vice versa, and therefore have great potential for future multifunctional device applications. The *macroscopic* ME effects have their *microscopic* origin from the interplay between the lattice degree of freedom and spin degree freedom. Neutron scattering,¹¹ as well as first-principles calculations^{12,13} shows that the improper ferroelectricity in TbMn₂O₅ is driven by the non-central symmetric magnetic ordering, which, by coupling to the lattice, lower the crystal symmetry.^{11,12} The spin-lattice coupling can also modify the lattice dynamic properties. Indeed, recent temperature dependent Raman measurements¹⁴ show anomalous phonon shift at T* ~ 1.5 T_N and near the magnetic phase transition temperature T_N in DyMn₂O₅. Similar anomalies are also observed for the IR modes.¹⁵ Further B-field dependent measurements show that the IR modes are very sensitive to local magnetic structure,¹⁶ which suggest that the spin-phonon coupling in this compound is very strong. However, the experiments give only the overall effects, and the detailed mechanism of the spin-phonon coupling is still lack.

First principles method has been applied successfully in studying spin-phonon coupling in geometrically frustrated spinel ZnCr₂O₄.¹⁷ It is a challenge problem to study the spin-phonon coupling in the spin frustrated systems, such as RMn₂O₅, because in these materials, the magnetic interactions are of different magnitudes (e.g., $|J_4|, |J_5| \gg |J_3|$),^{11,13} and the spin frustration leads to

complicated spin-spin correlations as functions of temperature and magnetic field. Therefore, the spin will develop different short range ordering at different temperature above the magnetic phase transition, and make it hard to identify the origin of the phonon anomalies.¹⁴ In this work, we study the spin-phonon coupling in DyMn₂O₅, to shed some light on the observed phonon anomalies. We show that the short range spin correlation and local spin structure have significant effects to the phonons frequencies in this material.

II. METHODOLOGY

The first-principles density-functional (DF) calculations are done by using the Vienna *ab initio* Simulations Package (VASP).^{18,19} We use a spin-polarized generalized gradient approximation (GGA), with Perdew-Burke-Ernzerhof functional.²⁰ A plane-wave basis and projector augmented-wave (PAW) pseudopotentials²¹ are used, with Mn *3p3d4s*, and Dy *5p5d6s* electrons treated self-consistently. A 500 eV plane-wave cutoff results in good convergence of the total energies. We relax the structure until the changes of total energy in the self-consistent calculations are less than 10⁻⁷ eV, and the remaining forces are less than 1 meV/Å. DyMn₂O₅ undergo several magnetic phase transitions⁵ at low temperature. We are interested in the phonon properties in the paramagnetic (PM) and anti-ferromagnetic (AFM) phase. To accommodate the magnetic structure, we use a 2×1×1 supercell.¹² For the supercell we used, a 1×2×4 Monkhorst-Pack k-points mesh converges very well the results.

III. RESULTS AND DISCUSSION

The fully relaxed DyMn₂O₅ is an AFM insulator, and has same lattice structure to that of TbMn₂O₅,^{12,22} both are of *Pb21m* symmetry, as Tb and Dy are isovalent. The lattice structure is distorted from a *Pbam* high (*H*) symmetry structure, due to the spin-lattice coupling.¹² The

*corresponding author, Email address: helx@ustc.edu.cn

TABLE I: Calculated phonon frequencies of ground state structure L . The experiment vaules for Raman phonons are extracted from Ref. 14, whereas the IR phonons frequencies are extracted from Ref. 16.

B_{2u}		A_g		B_{2g}		A_u		B_{3u}		B_{1g}		B_{1u}		B_{3g}	
GGA	Exp.	GGA	Exp.	GGA	Exp.	GGA	Exp.	GGA	Exp.	GGA	Exp.	GGA	Exp.	GGA	Exp.
671.8	680.0	679.2	695.0	566.0		614.1		677.2	713.0	683.7	675.0	607.2		557.2	585.0
628.4		617.7	625.0	480.8	510.0	531.2		620.1		647.0		530.0		507.9	495.0
553.4		615.0		470.8		499.5		597.1		588.3		497.9		471.7	
535.8		531.5	545.0	452.3	460.0	429.1		512.7	519.0	547.5	540.0	437.2		450.4	440.0
473.8		491.7	500.0	444.7		402.3		475.6		521.2		410.6	403.0	430.5	
438.0		444.2	460.0	336.5		287.5		465.5		470.1	485.0	296.7	290.0	324.7	320.0
412.1		407.2	420.0	293.0	305.0	225.7		378.3		411.0	420.0	249.3		289.8	
351.0		336.9	350.0	273.6		132.5		351.5		371.3	330.0	142.5		264.5	
314.4		311.1		230.7	220.0	110.8		317.0		299.6		-2.0		241.5	
267.8	267.0	235.4		209.6				265.4		242.6	235.0			189.8	
223.0		224.2	215.0	96.6				216.3	217.0	220.2	205.0			103.6	
163.2		136.4						158.2		171.9					
157.5		108.4						151.5		146.1	145.0				
99.6	100.0							111.6							

calculated lattice constants are $a=7.270$ Å, $b=8.518$ Å and $c=5.600$ Å, respectively, and are in very good agreement in experimental values⁵ (7.285, 8.487 and 5.668 Å respectively). The lattice constants are somewhat smaller than those of TbMn_2O_5 .^{12,22} Like TbM_2O_5 ,^{4,12} DyMn_2O_5 has two energetically degenerate lattice (and magnetic) structures, L and R , in which Mn^{4+} form an AFM square lattice in the ab plane, whereas Mn^{3+} couples to Mn^{4+} either antiferromagnetically via J_4 along a axis or with alternating sign via J_3 along b axis. Mn^{3+} ions in two connected pyramids also couple antiferromagnetically through J_5 . Here, we adopt the notations J_3 , J_4 and J_5 from Ref. 4, and define the J_3 to be the Mn^{4+} - Mn^{3+} superexchange interaction through pyramidal base corners, and J_4 the superexchange interaction through the pyramidal apex.

We first calculate all zone-center optical phonon frequencies of the fully relaxed structure (L or R) via a frozen-phonon technique,¹² and the results are listed in Table I. Symmetry analysis¹³ shows that for the high symmetry ($Pbam$) structure H , phonons belong to 8 irreducible representations (irreps), among them B_{1u} , B_{2u} and B_{3u} are IR active, where B_{1g} , B_{2g} , B_{3g} and A_g are Raman active and A_u is silent. However, in the low symmetry ($Pb21m$) structure (L or R), the Raman and IR modes couple to each other, and regroup to 4 irreps, i.e.,

$A_1 = B_{2u} \oplus A_g$; $A_2 = B_{2g} \oplus A_u$; $B_2 = B_{3u} \oplus B_{1g}$; $B_1 = B_{1u} \oplus B_{3g}$. The couplings between irreps. are very small, therefore the results are given by their major symmetry characters. As we see from Table I, the results are in excellent agreement with experiments.^{14,16} The calculated phonon frequencies are very close to those of TbMn_2O_5 , because Tb and Dy are isovalent and the two materials have very similar lattice structures. The inner products between the corresponding phonon modes²³ of the two compounds are close to unity, suggesting that they have very similar mode patterns.

Experimentally, there are several anomalies found for both Raman modes and IR modes, near the magnetic phase transitions. For example, anomalous phonon shift for the Raman modes had been observed at $T^* \sim 60-65$ K, and near the Néel temperature T_N .¹⁴ The highest A_g mode show a steep hardening upon cooling between T^* and T_N .¹⁴ For the IR modes, it has been found near 60K, the infrared active modes soften and several modes soften substantially.¹⁵ The phonon modes are also found to be very sensitive to the applied magnetic field.¹⁶ The observed phonon anomalous phonon shift strongly suggest that the spin-phonon coupling in this material is very strong.

Theoretically, the spin-lattice coupling in this compound can be described via an effect Hamiltonian,¹³

$$E(\{u_\lambda\}) = (E_0 - \sum_{ij} J_{ij} \mathbf{S}_i \cdot \mathbf{S}_j) - \sum_{ij} \sum_{\lambda} \frac{\partial J_{ij}}{\partial u_\lambda} u_\lambda \mathbf{S}_i \cdot \mathbf{S}_j + \left(\frac{1}{2} \sum_{\lambda} m_\lambda \omega_\lambda^2 u_\lambda^2 - \sum_{ij} \sum_{\lambda\rho} \frac{\partial^2 J_{ij}}{\partial u_\lambda \partial u_\rho} u_\lambda u_\rho \mathbf{S}_i \cdot \mathbf{S}_j \right), \quad (1)$$

where u_λ is the λ -th zone-center phonon, and \mathbf{S}_i is the magnetic moment of the i -th atom. Here, we consider

only the magnetic moments of the Mn^{3+} and Mn^{4+} ions. J_{ij} is the exchange interaction between two adjacent Mn

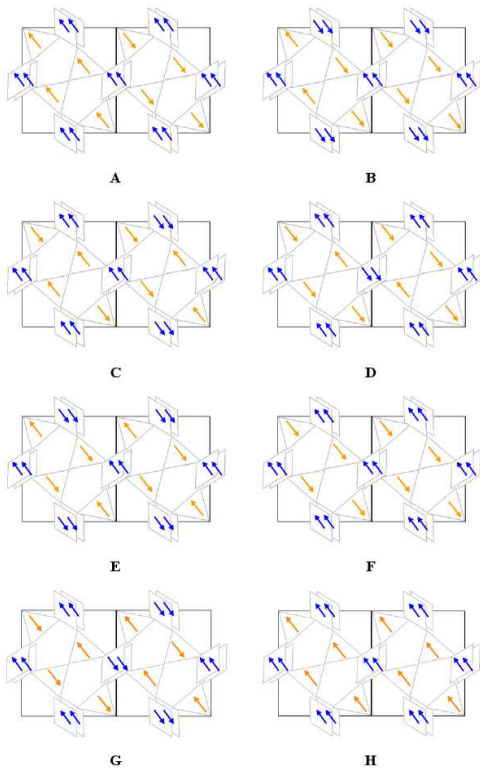


FIG. 1: (Color online) The spin configurations used in calculating phonon frequencies of different spin states.

ions. E_0 is the total energy of high symmetry structure H without spin-spin interactions, where the ground state spin configuration is determined by the first term. ω_λ is the frequencies of the λ -th phonon, calculated in the high symmetry PM state. The spin-lattice coupling have two effects: (i) The second term, which is linear in u , breaks the inversion symmetry of the system, and drive the structure to a low symmetry polarized state leading to coexistence of AFM and ferroelectricity. The coupling strength is proportional to $\partial J_{ij}/\partial u_\lambda$. However, this term would not change the phonon frequencies (at least to the first order approximation). (ii) The phonon modes ω_λ (including frequencies and eigenvectors) are modified in the presence of spin-phonon interaction, due to the third term of Eq. (1), where the spin-phonon coupling strength is $\partial^2 J_{ij}/\partial u_\lambda \partial u_\rho$. Different spin configuration (SC) $\{\mathbf{S}_i\}$ would therefore have different phonon frequencies.

To investigate how the SCs change the phonons in DyMn_2O_5 , we calculate the phonons frequencies of different SCs including the high temperature PM state, the AFM state, and the ferromagnetic (FM) state. The spin-lattice coupling strength J'' can be extracted by comparing the force-constant matrices calculated from these different spin states.¹⁷ [see Eq. (1)]. In this work, we focus on the B_{2u} and A_g modes, whereas other modes can be studied in similar way. To simplify the discussion,

all following calculations are done in the high symmetry structure H , constructed via symmetrizing structures L and R according to the $Pbam$ symmetry.¹² In reality, the lattice constants would be somewhat different at different SCs. In the present calculations, this effect is ignored and the lattice constants are fixed in the calculations.

The phonon frequencies of PM, AFM (SC G in Fig. 1) and FM (SC H in Fig. 1) states are compared in Table II for the A_g modes and in Table III for the B_{2u} modes. One may attempt to calculate the phonon frequencies of the PM state using spin *unpolarized* GGA, which is listed in the column under *u*-GGA. A quick look reveals that the phonon frequencies in this column are significantly lower than those of AFM and FM state. Especially, as shown in Table II, the A_g irrep has a soft mode, causing a Jahn-Teller distortion.²⁴ The phonon frequencies calculated from *u*-GGA is not a good approximation for the PM state, because the Mn ions have local magnetic moments even in the PM phase, although their directions are distributed randomly. Alternatively, we calculate $\langle \omega \rangle_{dis}$, which are the averaged phonon frequencies of several fully disordered SCs (A, B, C in Fig. 1) so all exchange interactions are canceled out. The averaged phonon frequencies $\langle \omega \rangle_{dis}$ are close to those of the AFM and FM states without soft phonons.

However, the spins are fully disordered only at very high temperature. At lower temperature, especially close to the magnetic phase transition, the spins are somehow correlated, and develop short range ordering. Since J_4 is the largest among all the exchange interactions,¹³ to compare with experiments, we consider the ordering of J_4 interactions. We calculate $\langle \omega \rangle_{J_4}$, which are the averaged phonon frequencies of three SCs (D, E, F in Fig. 1) in which J_4 are fixed in the AFM configuration, whereas all other exchange interactions are canceled out. As we see from Table II and Table III, the frequencies of most modes in different SCs differ by about 3 - 5 cm^{-1} , which are of similar magnitude to the phonon shifts in the magnetic field experiment.¹⁶ However, the high frequency B_{2u} (671 cm^{-1}) and A_g (679 cm^{-1}) modes change dramatically ($\sim 20 \text{ cm}^{-1}$) for different SCs. Especially, $\langle \omega \rangle_{dis}$ and $\langle \omega \rangle_{J_4}$ are different by about 10 and 13 cm^{-1} for the A_g and B_{2u} modes, respectively, though both belong to the PM phase. Interestingly, the two modes frequencies of $\langle \omega \rangle_{J_4}$ are close to the those in AFM state, and $\langle \omega \rangle_{dis}$ have the mean values of those of AFM and FM states. It is usually believed that GGA overestimates the exchange interactions, whereas including the on-site Coulomb correlation may improve this problem. To see how including the on-site Coulomb correlation will change the spin-phonon coupling in DyMn_2O_5 , we have carried out GGA + U calculations of the phonons in different SCs. The on-site Coulomb U of Mn ions has been taken to be a reasonable value 4.0 eV, whereas the exchange parameter $j=0.8$ eV is used. The results are also listed in Table II and Table III for the A_g and B_{2u} modes respectively. As we see, GGA + U significantly overestimates the frequencies of the high frequency modes when compared to experi-

TABLE II: The A_g modes calculated in high symmetry structure H of different spin configurations using GGA and GGA + U methods.

u	-GGA		GGA		GGA + U			
	$\langle\omega\rangle_{dis}$	$\langle\omega\rangle_{j4}$	AFM	FM	$\langle\omega\rangle_{dis}$	$\langle\omega\rangle_{j4}$	AFM	FM
571.1	667.7	677.6	679.0	662.8	746.1	759.9	759.9	723.2
563.2	621.5	625.8	618.6	629.7	658.8	661.3	659.4	653.4
530.7	617.7	618.4	613.5	617.3	634.2	635.3	631.0	638.3
463.3	537.2	540.9	531.1	547.0	559.3	561.1	556.6	562.2
432.9	490.6	492.2	491.3	494.1	505.4	506.3	506.0	506.4
409.2	441.0	442.8	442.6	441.4	451.4	452.7	452.6	450.1
369.6	414.3	407.9	407.0	429.8	438.2	436.6	436.0	440.3
249.6	340.0	337.6	337.6	340.3	342.6	342.3	341.6	343.0
178.8	321.9	329.2	311.0	331.7	328.9	331.9	323.2	334.8
152.7	238.7	237.2	236.2	243.9	248.3	248.0	247.5	249.2
102.9	222.3	220.2	219.6	225.9	217.7	216.9	216.6	220.1
66.1	136.8	137.5	136.0	137.6	141.1	141.6	140.9	141.0
-174.2	110.0	110.0	109.3	111.2	113.2	113.4	113.1	113.5

TABLE III: The B_{2u} modes calculated in high symmetry structure H of different spin configurations using GGA and GGA + U methods.

u	-GGA		GGA		GGA + U			
	$\langle\omega\rangle_{dis}$	$\langle\omega\rangle_{j4}$	AFM	FM	$\langle\omega\rangle_{dis}$	$\langle\omega\rangle_{j4}$	AFM	FM
586.4	660.2	673.3	671.7	649.6	723.7	736.6	735.9	705.8
512.8	627.2	625.5	626.1	623.8	659.1	659.4	659.1	657.9
507.2	551.6	552.2	553.4	552.3	578.5	578.7	579.4	577.9
488.7	534.0	530.9	535.3	534.1	566.6	567.0	568.3	564.6
431.2	474.5	473.5	475.7	476.4	495.5	494.5	495.6	498.1
391.0	439.5	437.2	439.2	438.1	461.8	462.0	462.2	459.4
381.3	409.7	410.0	411.7	406.0	419.9	420.2	420.9	418.0
310.0	353.6	350.2	350.8	357.6	365.7	364.9	365.2	366.1
274.3	315.0	314.3	315.2	314.6	316.2	315.8	316.3	316.6
257.7	272.7	266.0	267.9	280.1	283.8	282.5	282.5	285.5
211.1	222.2	221.8	223.4	220.8	211.7	212.0	212.5	212.7
142.6	162.0	162.2	162.0	161.4	165.6	165.7	165.5	165.7
139.2	156.8	156.9	157.0	157.3	163.3	163.5	163.7	162.7
93.9	98.4	98.6	99.2	96.8	94.0	94.3	94.6	93.4

ments. However, the frequency difference between different SCs are almost remain the same to those without U , suggesting that the spin-phonon coupling constants do not change much by including the on-site Coulomb correlation. In the following discussion, we therefore focus only the GGA results.

To understand the results, we analyze the vibrational pattern of the two modes, shown in Fig. 2. For the high-frequency A_g mode, about 90% of the vibration is associated with O_3 (the oxygens that connect Mn^{3+} and Mn^{4+} along the a axis, and convey J_4 interaction). The O_3 atoms vibrate in the ab plane, with an angle of 21.4° to a axis. This mode also has small components of Mn^{3+} vibrating in the a -axis, and Mn^{4+} motion in the c -axis. Therefore J_5 may also affect the A_g mode (but considerably smaller than J_4). In the high-frequency B_{2u} mode, more than 70% of the contribution comes from O_3 , which also vibrate in the ab plane, with an angle of 19.9° to a

axis. The rest contribution includes the motion of Mn^{4+} along a axis. If the spin exchange interaction is local, the motion the O_3 atoms would only tune the J_4 interactions. Therefore the J_4 interaction plays an essential role of the spin-phonon coupling in these two modes. Now it is easy to understand the phonon shifts of the two modes in different SCs. According to Eq. (1), the frequency shifts of the highest A_g and B_{2u} modes are $\langle\mathbf{S}_3 \cdot \mathbf{S}_4\rangle \partial^2 J_4 / \partial u_\lambda^2$, where \mathbf{S}_3 , \mathbf{S}_4 are the spin vectors of Mn^{3+} and Mn^{4+} ions associated with J_4 , respectively. For the fully disordered SC, $\langle\mathbf{S}_3 \cdot \mathbf{S}_4\rangle=0$. In the J_4 short range ordered state and in AFM state $\langle\mathbf{S}_3 \cdot \mathbf{S}_4\rangle=-S_3 S_4$, whereas in FM state, $\langle\mathbf{S}_3 \cdot \mathbf{S}_4\rangle=S_3 S_4$. $S_3=2.3 \mu_B$ and $S_4=1.64 \mu_B$, are the local magnetic moments. By comparing the force-constant matrices of different SCs, we estimate $\partial^2 J_4 / \partial u_\lambda^2 \sim 0.120$ meV/ $(\text{\AA} \cdot \mu_B)^2$ for the two high frequency modes. As discussed in previous section, this value remain unchanged when including the on-site Coulomb interactions.

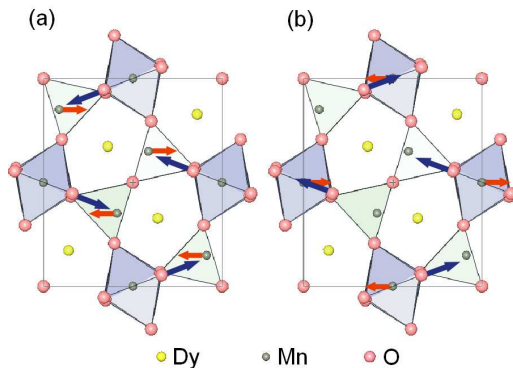


FIG. 2: (Color online) The mode pattern of the highest (a) A_g mode and (b) B_{2u} mode.

Experimentally, such large phonon hardening due to J_4 ordering was not directly observed during the temperature dependent measurement^{14,15} for two reasons. First, the J_4 ordering develop gradually with decreasing of the temperature. A Monte Carlo simulation²⁵ show that the average of $\langle \mathbf{S}_3 \cdot \mathbf{S}_4 \rangle$ increases from 80% to 90% of its maximum value when temperature lower from 1.5 T_N to T_N . Second, the phonon frequencies hardening due to J_4 ordering is accompanied by the anharmonic effects,^{14,15} and it is hard to isolate the anharmonic effects and spin-phonon effects in experiments. The lower frequencies modes involve collective motion of many atoms. Therefore, the phonon frequency shifts due to spin-phonon cou-

pling are a consequence of the competition of many J'' s, and are much smaller than the high frequency modes.

Below Néel temperature, T_N , the material is in the long range ordered AFM state. We then compare the phonon frequencies of short range ordered state $\langle \omega \rangle_{J_4}$ to those of AFM state. As we see, while the highest A_g mode hardens by 2 cm^{-1} , and the highest B_{2u} mode softs by 2 cm^{-1} , consistent with experiments.^{14,15} The frequencies difference between $\langle \omega \rangle_{J_4}$ and AFM might come from the J_5 interactions.

IV. SUMMARY

To summarize, we have investigated the spin-phonon coupling in a spin frustrated DyMn_2O_5 system via first-principles calculations. We compare the phonon modes calculated from different spin configurations. The results show that the short range spin ordering can dramatically change the phonon frequencies in this compound, and might be responsible for the observed phonon anomalies near and above the magnetic phase transitions.

We would like to thank J. L. Musfeldt and J. Cao for communicating results prior to publication. L.H. acknowledges the support from the Chinese National Fundamental Research Program 2006CB921900, the Innovation funds and ‘‘Hundreds of Talents’’ program from Chinese Academy of Sciences, and National Natural Science Foundation of China.

-
- ¹ T. Kimura, T. Goto, H. Shintani, K. Ishizaka, T. Arima, and Y. Tokura, *Nature(London)* **426**, 55 (2003).
 - ² T. Goto, T. Kimura, G. Lawes, A. P. Ramirez, and Y. Tokura, *Phys. Rev. Lett.* **92**, 257201 (2004).
 - ³ N. Hur, S. Park, P. A. Sharma, J. S. Ahn, S. Guha, and S.-W. Cheong, *Nature (London)* **429**, 392 (2004).
 - ⁴ L. C. Chapon, G. R. Blake, M. J. Gutmann, S. Park, N. Hur, P. G. Radaelli, and S. W. Cheong, *Phys. Rev. Lett.* **93**, 177402 (2004).
 - ⁵ G. R. Blake, L. C. Chapon, P. G. Radaelli, S. Park, N. Hur, S.-W. Cheong, and J. Rodriguez-Carvajal, *Phys. Rev. B* **71**, 214402 (2005).
 - ⁶ N. Hur, S. Park, P. A. Sharma, S. Guha, and S.-W. Cheong, *Phys. Rev. Lett.* **93**, 107207 (2004).
 - ⁷ R. ValdesAguilar, A. B. Sushkov, S. Park, S. W. Cheong, and H. D. Drew, *Phys. Rev. B* **74**, 184404 (2006).
 - ⁸ S.-W. Cheong and M. Mostovoy, *Nature Materials* **6**, 13 (2007).
 - ⁹ H. Katsura, N. Nagaosa, and A. V. Balatsky, *Phys. Rev. Lett.* **95**, 057205 (2005).
 - ¹⁰ I. A. Sergienko and E. Dagotto, *Phys. Rev. B* **73**, 094434 (2006).
 - ¹¹ L. C. Chapon, P. G. Radaelli, G. R. Blake, S. Park, and S.-W. Cheong, *Phys. Rev. Lett.* **96**, 097601 (2006).
 - ¹² C. Wang, G.-C. Guo, and L. He, *Phys. Rev. Lett.* **99**, 177202 (2007).
 - ¹³ C. Wang, G.-C. Guo, and L. He, *Phys. Rev. B* **77**, 134113 (2008).
 - ¹⁴ A. F. García-Flores, E. Granado, H. Martinho, R. R. Urbano, C. Rettori, E. I. Golovenchits, V. A. Sanina, S. B. Oseroff, S. Park, et al., *Phys. Rev. B* **73**, 104411 (2006).
 - ¹⁵ J. Cao, L. I. Vergara, J. L. Musfeldt, A. P. Litvinchuk, Y. J. Wang, S. Park, and S.-W. Cheong, *Phys. Rev. B* **78**, 064307 (2008).
 - ¹⁶ J. Cao, L. I. Vergara, J. L. Musfeldt, A. P. Litvinchuk, Y. J. Wang, S. Park, and S.-W. Cheong, *Phys. Rev. Lett.* **100**, 177205 (2008).
 - ¹⁷ C. J. Fennie and K. M. Rabe, *Phys. Rev. Lett.* **96**, 205505 (2006).
 - ¹⁸ G. Kresse and J. Hafner, *Phys. Rev. B* **47**, 558 (1993).
 - ¹⁹ G. Kresse and J. Furthmuller, *Phys. Rev. B* **54**, 11169 (1996).
 - ²⁰ J. P. Perdew, K. Burke, and M. Ernzerhof, *Phys. Rev. Lett.* **77**, 3865 (1996).
 - ²¹ P. E. Blochl, *Phys. Rev. B* **50**, 17953 (1994).
 - ²² J. A. Alonso, M. T. Casais, M. J. Martinez-Lope, J. L. Martinez, and M. T. Fernandez-Diaz, *J. Phys.: Condens. Matter* **9**, 8515 (1997).
 - ²³ L. He, J. B. Neaton, D. Vanderbilt, and M. H. Cohen, *Phys. Rev. B* **67**, 012103 (2003).
 - ²⁴ C. Kittel, *Introduction to Solid State Physics, 7th edition* (John Wiley & Sons, 1996).
 - ²⁵ K. Cao and L. He, (unpublished).